

# Final Report

Several types of the GaSb-based type-I quantum well (QW) diode lasers were designed and fabricated. World record parameters were demonstrated for all devices. High power 1.95 $\mu$ m type-I quantum-well GaSb-based diode lasers were used to pump fluoride glass holmium doped fiber laser with record power conversion efficiency.

The report contained three parts: (a) development of the pump diode lasers; (b) demonstration of the diode pumped Ho-doped fiber laser; and (c) development of 2.7 and 3.15  $\mu$ m diode lasers operating at room temperature in continuous wave regime. The part (a) will be described firstly and then details of the part (b) will be given after the characteristics of the pumping diodes are presented. Part (c) will describe the progress in development of the high power and diffraction limited sources with increased wavelength.

## (a). Development of the 1.9 – 2.3 $\mu$ m GaSb-based type-I quantum-well diode lasers.

High-power diodes emitting in spectral region from 1.9 to 2.5  $\mu$ m are required for variety of medical, industrial and military applications. Medical applications include aesthetic or other surgery as well as infrared nerve stimulation. Industrial applications include material processing, for instance, transparent plastic welding as well as optical pumping of the various laser hosts and nonlinear wavelength converters. High power narrow spectrum lasers are required to seed the cavity of high energy lasers for laser detection and ranging. Tunable devices find applications for absorption spectroscopy of CO<sub>2</sub>, CO, etc. Resonant or nearly resonant optical pumping of the chromium doped II-VI semiconductors, novel type-II quantum well Sb-based semiconductors, and holmium doped crystals, glasses and fibers can be achieved. The resonant pumping of the holmium doped fiber laser was demonstrated in this work.

### (a).1. High power ~2.2 $\mu$ m lasers with broadened waveguide design.

Studies on the role of compressive strain above 1 % on the threshold and efficiency of GaSb-based diode lasers have been performed previously [1,2]. It was demonstrated that increasing the compressive strain from 1 to 1.5 % in GaInAsSb QWs improves both the differential gain and the threshold current density of diode lasers. Both heavy-light hole splitting and reduced As composition in heavily strained QW shift the valence band edge upward. We advocate that the increased valence band offset between the heavily compressively strained GaInAsSb QWs and the AlGaAsSb barrier layers is responsible for the observed enhancement of the device performance parameters. It is also important to use relatively narrow QWs (~ 10 nm or narrower) to maintain sufficient separation between topmost heavy hole subbands. The mechanism of improvement is related to the reduced thermal population of the barrier and second subband states and the resulting decrease of the threshold carrier concentration. The reduction of the threshold carrier concentration results from both the decreased transparency carrier concentration and increased differential gain. In this work, we demonstrate this active region design approach with the fabrication of 2.2  $\mu$ m high power diode lasers and their arrays.

Figure 1 shows schematically the flat band diagram of the central part of broadened waveguide heterostructure of 2.2  $\mu$ m emitting high power diode lasers [3]. The laser heterostructure was grown by solid-source molecular beam epitaxy (MBE) on Te-doped GaSb substrates in a Veeco GEN-930 modular system equipped with valved cracker cells for As and Sb. All layers except for QWs were lattice matched to the substrate.

Report Documentation Page			Form Approved OMB No. 0704-0188	
<p>Public reporting burden for the collection of information is estimated to average 1 hour per response, including the time for reviewing instructions, searching existing data sources, gathering and maintaining the data needed, and completing and reviewing the collection of information. Send comments regarding this burden estimate or any other aspect of this collection of information, including suggestions for reducing this burden, to Washington Headquarters Services, Directorate for Information Operations and Reports, 1215 Jefferson Davis Highway, Suite 1204, Arlington VA 22202-4302. Respondents should be aware that notwithstanding any other provision of law, no person shall be subject to a penalty for failing to comply with a collection of information if it does not display a currently valid OMB control number.</p>				
1. REPORT DATE <b>31 AUG 2011</b>	2. REPORT TYPE	3. DATES COVERED <b>01-03-2008 to 31-05-2011</b>		
4. TITLE AND SUBTITLE <b>Holmium Doped Solid State Laser Resonantly Pumped And Q-Switched By Novel GaSb-Based Photonic Devices</b>		5a. CONTRACT NUMBER		
		5b. GRANT NUMBER		
		5c. PROGRAM ELEMENT NUMBER		
6. AUTHOR(S)		5d. PROJECT NUMBER		
		5e. TASK NUMBER		
		5f. WORK UNIT NUMBER		
7. PERFORMING ORGANIZATION NAME(S) AND ADDRESS(ES) <b>State University of New York at Stony Brook, Department of Electrical and Computer Engineering, Stony Brook, NY, 11794</b>		8. PERFORMING ORGANIZATION REPORT NUMBER <b>; AFRL-OSR-VA-TR-11-066</b>		
9. SPONSORING/MONITORING AGENCY NAME(S) AND ADDRESS(ES)		10. SPONSOR/MONITOR'S ACRONYM(S)		
		11. SPONSOR/MONITOR'S REPORT NUMBER(S) <b>AFRL-OSR-VA-TR-11-066</b>		
12. DISTRIBUTION/AVAILABILITY STATEMENT <b>Approved for public release; distribution unlimited</b>				
13. SUPPLEMENTARY NOTES				
14. ABSTRACT <p>A highly efficient Ho<sup>3+</sup>-doped fluoride glass fiber laser operating at 2.08 ?m is demonstrated using nearly resonant pumping at 1.94 ?m by GaSb-based diode lasers. A maximum slope efficiency of 78% and output power above 500 mW were obtained. Asymmetric laser heterostructure was developed to improve beam properties of GaSb-based diode lasers. Multimode 100-?m-wide ridge waveguide lasers with ~40 degrees fast axis beam divergence demonstrated output power of about 1.5 W CW at 20 C. High-power 2.2 ?m broadened waveguide diode lasers demonstrate internal optical loss below 4 cm<sup>-1</sup>, threshold current density below 100 A/cm<sup>2</sup> and CW output power of 1.6 W. Linear laser arrays generated above 25 W of quasi-CW output power. The device power conversion efficiencies were better than 20% in peak and above 10% at maximum output power level. Diode lasers operating at 2.7 ?m with room-temperature CW output power of 600 mW and peak power-conversion efficiency of 10% were demonstrated. Ridge waveguide diode lasers operating in the spectral region near 3.15 ?m demonstrated single spatial mode CW output power of 9 mW at 20 C and operated up to 40 C in CW regime.</p>				
15. SUBJECT TERMS				
16. SECURITY CLASSIFICATION OF:			17. LIMITATION OF ABSTRACT <b>Same as Report (SAR)</b>	18. NUMBER OF PAGES <b>22</b>
a. REPORT <b>unclassified</b>	b. ABSTRACT <b>unclassified</b>	c. THIS PAGE <b>unclassified</b>	19a. NAME OF RESPONSIBLE PERSON	

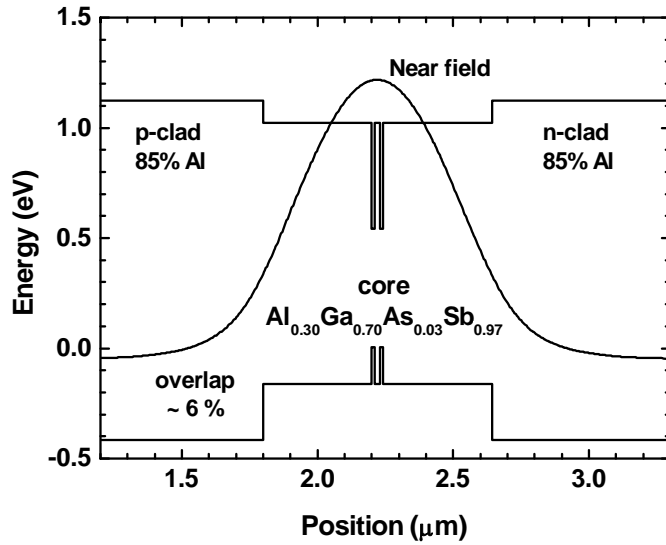


**Figure 1.** Calculated band diagram of the laser heterostructure overlaid with the near field optical mode distribution.

Heavily doped graded bandgap layers were introduced between the n(p)-GaSb buffer(cap) layers and the n(p)-Al<sub>0.85</sub>Ga<sub>0.15</sub>As<sub>0.07</sub>Sb<sub>0.93</sub> cladding layers. The claddings were 1.5  $\mu\text{m}$  thick and were doped with Te (nominal  $n = 10^{18} \text{ cm}^{-3}$ ) and Be (nominal  $p = 10^{17} \text{ cm}^{-3}$  for the first 500 nm adjacent to the waveguide core and  $10^{18} \text{ cm}^{-3}$  for the remaining 1  $\mu\text{m}$ ). Lower than nominal n-doping levels are expected in quaternary aluminum-containing alloys. The waveguide core was composed of a dual-QW active region centered between 400-nm-thick nominally undoped Al<sub>0.3</sub>Ga<sub>0.7</sub>As<sub>0.03</sub>Sb<sub>0.97</sub> layers. The QWs were 11 nm thick Ga<sub>0.72</sub>In<sub>0.28</sub>As<sub>0.03</sub>Sb<sub>0.97</sub> with a compressive strain of 1.5 % separated by a 20 nm thick Al<sub>0.3</sub>Ga<sub>0.7</sub>As<sub>0.02</sub>Sb<sub>0.98</sub> barrier. The valence band offset between the QW and barrier materials was estimated to be adequate at about 150 meV, while the band offset in the conduction band is ample and in excess of 500 meV. Optical field calculations predicted the overlap of the laser mode with the p-cladding to be about 6%, resulting in low optical losses in these broadened waveguide lasers.

The laser wafer was processed into an index guided ridge waveguide structure by wet etching of the p-cladding layer outside of the 100  $\mu\text{m}$  wide current stripes. For CW characterization the bars were cleaved and immediately loaded to vacuum reactor to be coated to reflect 3 % (AR) at the front mirror and 95 % (HR) at the back mirror. The AR coating was single quarter wave layer of Al<sub>2</sub>O<sub>3</sub> while HR was two periods of a Si/Al<sub>2</sub>O<sub>3</sub> Bragg reflector. Both the individual devices and the linear laser arrays were In-soldered epi-side-down with flux onto gold-coated copper blocks. Top contacts were wire-bonded. CW characterization was performed with mounted devices bolted to a Peltier-cooled copper plate. The hot side of the Peltier was water-cooled. The cooling system was capable of removing about 100 W of heat. Laser output power was measured using a calibrated thermopile sensor with a 2 cm diameter aperture. The sensor was placed about 1 cm away from the laser output mirror and no collecting optics were used. Figure 2 shows the measured CW output powers and power conversion efficiencies of individual lasers at a heat sink temperature of 17 °C.

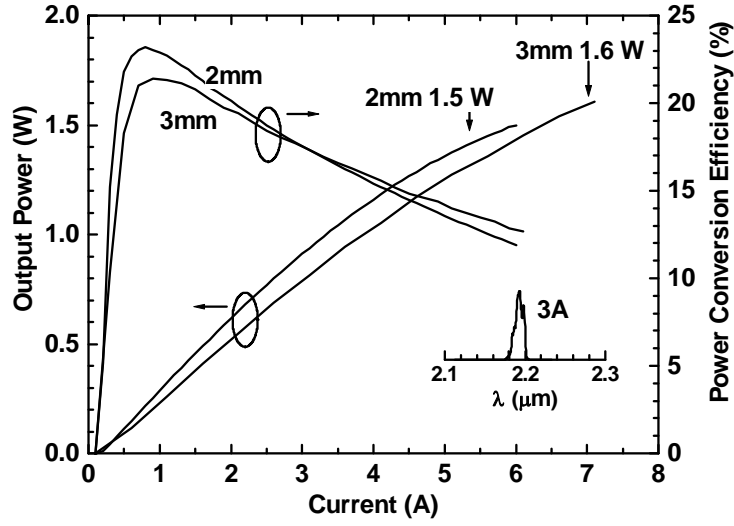


**Figure 2.** CW power and power conversion characteristics of single emitter  $2.2\mu\text{m}$  lasers with 2- and 3-mm-long cavities (AR/HR,  $17^\circ\text{C}$ ). Inset shows laser spectrum.

A CW output power of 1.5 W was reached at 6 A for the 2-mm-long 100- $\mu\text{m}$ -wide devices. Lasers with 3 mm long cavity length and, hence, increased thermal footprints generate 1.6 W at 7A despite reduced overall device efficiency. High power lasers demonstrate CW threshold current densities below  $100 \text{ A/cm}^2$ , i.e. less than  $50 \text{ A/cm}^2$  per QW. The threshold current density demonstrates excellent temperature stability as indicated by a  $T_0$  parameter above 90 K as measured in short pulse regime over a temperature range from 15 to  $60^\circ\text{C}$  for 1-mm-long uncoated devices. Device power conversion efficiency peaked at more than 20 % and remained above 10 % at the maximum output power level. CW external efficiency near threshold was above 50%. The temperature stability of the efficiency is characterized by a parameter  $T_1$  of about 290 K. The laser spectrum was centered near  $2.19 \mu\text{m}$  at a current of 3 A, with a full-width at half-maximum (FWHM) of 12 nm.

Optical gain spectra for several under threshold currents were measured using the Haki-Paoli method [4] with a Fourier transform spectrometer and external InSb detector (Figure 3). Amplified spontaneous emission collection and beam focusing on the photodetector were performed using reflective optics. A mechanical slit (about 1 mm) in front of the reflective objective ( $\text{NA} = 0.5$ ) was used to filter out the higher order lateral modes of the laser cavity. Total optical loss of  $15 - 16 \text{ cm}^{-1}$  can be estimated from long-wavelength part of the gain spectrum resulting into about  $4 \text{ cm}^{-1}$  value of the internal loss (mirror loss of about  $12 \text{ cm}^{-1}$  can be calculated for uncoated 1-mm-long lasers). This relatively low internal optical loss was achieved by waveguide broadening in combination with reduced doping of the p-cladding section adjacent to waveguide core. Transparency current density is only about  $20 \text{ A/cm}^2$  per QW. The net modal differential gain is above  $350 \text{ cm}^{-1}/\text{A}$ . Threshold is achieved when quasi-Fermi levels are separated by about 35 meV above bandgap (see gain width at threshold as measured at total loss level). The threshold is achieved at current density that is only about twice higher than that at transparency.

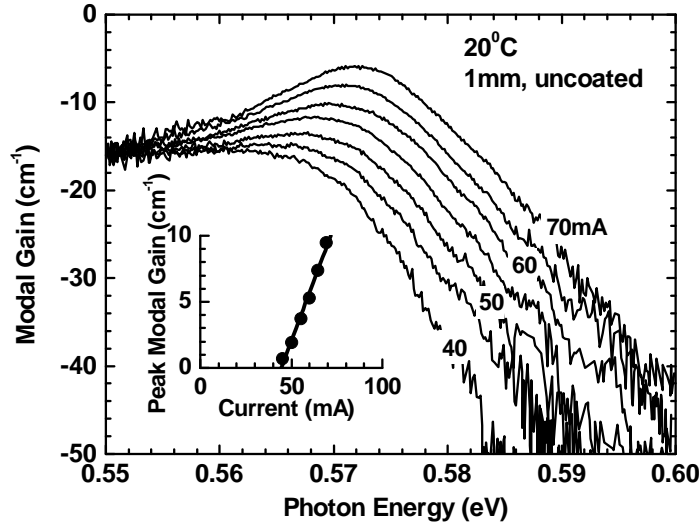


**Figure 3.** Current dependences of the modal gain spectra measured at  $20^{\circ}\text{C}$  for 1-mm-long uncoated devices. The inset shows the corresponding dependence of the peak modal gain on current.

The far field distributions were measured by scanning a single  $500\text{ }\mu\text{m}$  diameter photodetector at a distance of about 30 cm away from laser front mirror (Figure 4a). Divergence in the fast axis direction was typical for diffraction limited broadened waveguide lasers with a FWHM of about 63 degrees that is independent of current. The calculated fast axis far field distribution (from near field in Figure 1) had a beam divergence of about 62 degrees, i.e. in close correspondence to the experimental value. The multimode beam in the slow axis direction shows a far field divergence of about 10 degrees that tends to increase somewhat with current. The corresponding near field pattern clearly shows filamentation with an average filament spacing of about  $12\text{ }\mu\text{m}$  (Figure 4b).

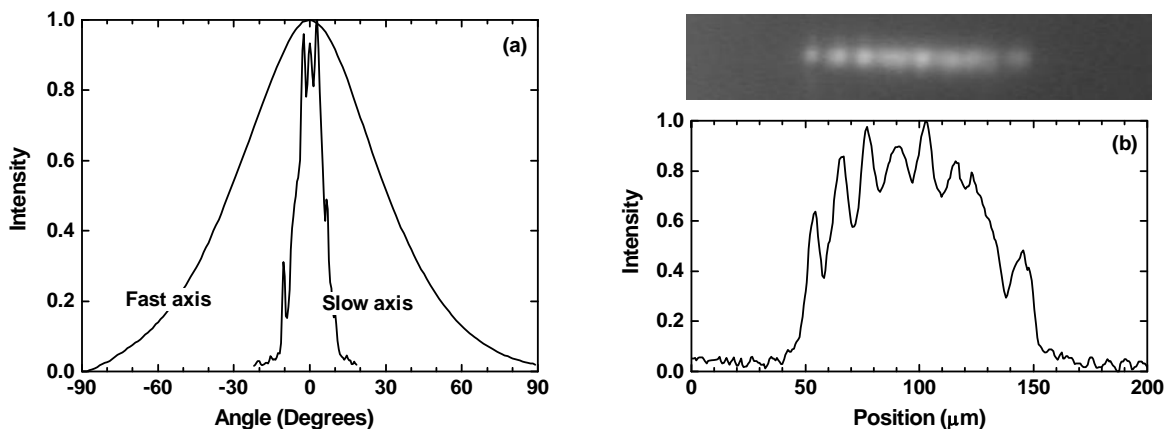


**Figure 4.** (a) Fast and slow axis far field distributions measured for 2-mm-long, AR/HR coated single emitter lasers; (b) Near field distribution measured for 1-mm-long, AR/HR coated lasers.

Figure 5 shows the measured CW power and power conversion characteristics of a 22 element 1-mm-long cavity linear laser array at a heat sink temperature of  $17^{\circ}\text{C}$ . The array fill-

factor was a conservative 20 %. Each laser element emitted through a 100  $\mu\text{m}$  wide aperture. The inset shows the near field image of the array output mirror. A CW output power of more than 12 W was reached at 50 A where power conversion efficiency is about 10 %. Saturation of the CW output power level is caused by the limitations of the Peltier cooler. The laser array spectrum experiences red shift and line broadening with current (see inset). At 40 A the output is centered at 2.23  $\mu\text{m}$  with a linewidth of about 20 nm. In the quasi-CW regime (30  $\mu\text{s}$ , 300Hz) the array output power reaches 27W at 90A.

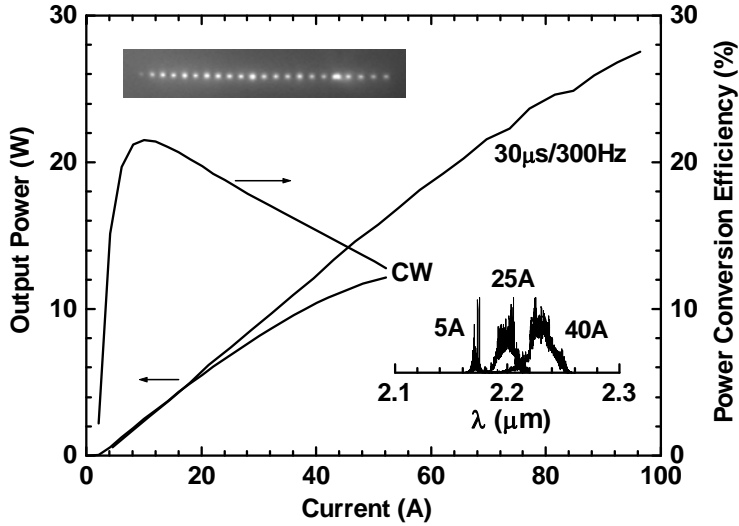


**Figure 5.** CW power and power conversion characteristics of 22 element 1-mm-long AR/HR coated laser array measured in CW and quasi-CW regimes at 17 °C. Insets show near field (top) and laser spectra (bottom).

### (a).2. High power ~2 $\mu\text{m}$ lasers with improved beam properties.

Beam divergence in excess of 60 degrees FWHM (Figure 4a) complicates fiber coupling and requires expensive optics with numerical aperture above 0.5. In order to improve device brightness the broadened waveguide design approach was abandoned. GaSb-based diode lasers with narrow symmetric waveguide and increased spot size in near field were developed previously [5]. High power CW operation with 1.96 W at 17 °C from 150- $\mu\text{m}$ -wide aperture (corresponds to about 1.3 W from 100- $\mu\text{m}$ -wide aperture) and fast axis beam divergence of 44 degrees FWHM was reported. Reduction of the beam divergence below 44 degrees can be achieved by further decrease of the waveguide core. However, it leads to enhanced interaction of the optical field with p-cladding and possibly even p-contact layers. The necessary modifications of the laser heterostructure are likely to increase electrical and thermal resistances of the device.

Asymmetric waveguide design can be utilized to reduce the fast axis beam divergence below 40 degrees FWHM. In laser heterostructures with asymmetric waveguide the beam quality can be improved [6] by spreading optical mode selectively into n-cladding but not into p-cladding. In this design the p-cladding thickness does not have to be increased to accommodate the mode interaction with heavily doped p-contact layers since penetration of the optical field into p-cladding is restricted. This is expected to benefit thermal transport in p-down mounted lasers. From our experience an increased overlap with n-cladding should not lead to substantial internal loss increase in contrast to increased overlap with p-cladding, presumably due to dominant role of inter valence band absorption [7]. Details of the conduction band structure of the particular

cladding material should be taken into account to accurately predict the contribution of the free electron absorption to total loss. In the specific structures used here the n-cladding composition resulted into material with three valleys in conduction band to have almost the same energy minimum so no inter valley resonances were expected. Hence no substantial increase of the internal loss could be expected in structures with optical field extended selectively into n-cladding of the particular composition.

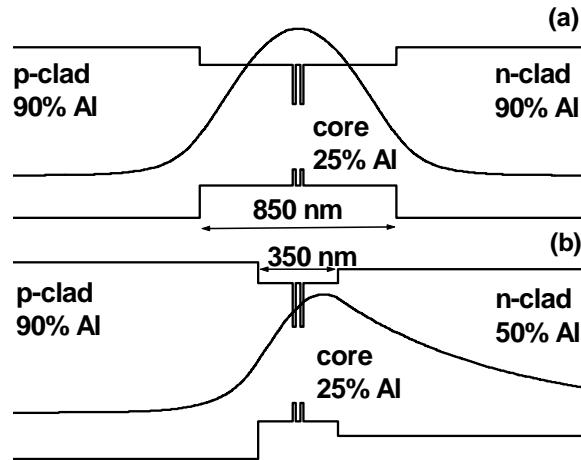
Previously diode lasers with very low output power below 50 mW and fast axis beam divergence of 30 degrees FWHM were obtained by developing laser heterostructure with asymmetric waveguide core [8]. In this work an asymmetric penetration of the modal field into p- and n-cladding was achieved by using different compositions of the cladding materials. The beam properties of the high power 2  $\mu\text{m}$  emitting GaSb-based diode lasers was improved by utilization of the waveguide structure with asymmetric claddings. The AlGaAsSb p-cladding contained about 85-90% of Al while n-cladding aluminum content was reduced to 45-50 %. Corresponding increase of refractive index led to modal spreading to n-cladding layer resulting into reduced fast axis beam divergence. Refractive index step between  $\text{Al}_{0.9}\text{Ga}_{0.1}\text{As}_{0.07}\text{Sb}_{0.93}$  claddings and  $\text{Al}_{0.25}\text{Ga}_{0.75}\text{As}_{0.02}\text{Sb}_{0.98}$  core in symmetric broadened waveguide laser structure 1 (Table 1) can be estimated as 0.45 for 2  $\mu\text{m}$  light [9]. Devices with asymmetric claddings and variable waveguide core thicknesses ranging from above 800 down to below 300 nm were designed, fabricated and characterized (Table 1).

	p-clad		core		n-clad	
	% Al	nm	% Al	nm	% Al	nm
1	90	1500	25	859	90	1500
2	90	1500	25	850	50	2000
3	90	1500	25	550	50	2000
4	90	1500	25	350	50	2000
5	90	1500	25	250	50	2500

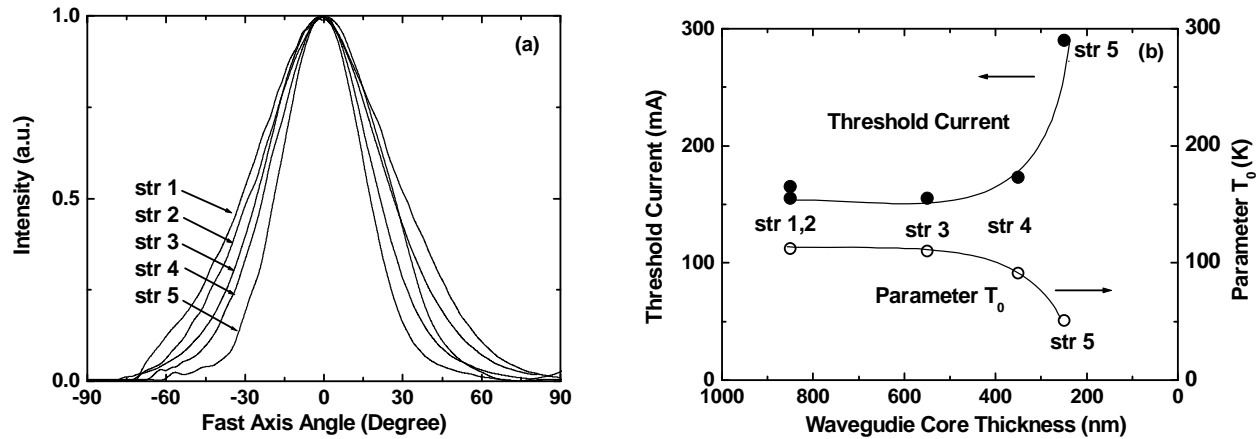
**Table 1.** Composition and width of the claddings and core layers of the 2  $\mu\text{m}$  emitting laser heterostructures studied.

Figure 6a plots schematically the calculated band alignment and near field distribution in typical reference symmetric broadened waveguide laser heterostructure [10]. Change of the composition of the n-cladding from  $\text{Al}_{0.9}\text{Ga}_{0.1}\text{As}_{0.07}\text{Sb}_{0.93}$  to  $\text{Al}_{0.5}\text{Ga}_{0.5}\text{As}_{0.03}\text{Sb}_{0.97}$ , reduces the refractive index step between n-cladding and waveguide core down to about 0.2. The resulting waveguide asymmetry leads to spreading of the laser mode into n-cladding but keeps overlap with p-cladding low (Figure 6b).

Reduction of the waveguide core width in laser structure with asymmetric claddings from 850 nm to 550 (structure 3), then to 350 (structure 4) and finally down to 250 nm (structure 5) is accompanied by gradual improvement of the beam quality. Figure 7a shows that the FWHM maximum of the far field reduces to below 40 degrees thanks to progressing expansion of the modal field into n-cladding direction.



**Figure 6.** Calculated band alignment diagram and transverse near field distribution of (a) symmetric broadened waveguide laser structure 1 and (b) asymmetric narrow waveguide laser structure 4.



**Figure 7.** (a) Measured fast axis far field distributions of 2  $\mu\text{m}$  emitting laser diodes with 1-mm-long, 100- $\mu\text{m}$ -wide uncoated cavities. Structure numbers correspond to table 1; (b) Dependences of the threshold current density at 20  $^{\circ}\text{C}$  and parameter  $T_0$  on waveguide core thickness. Measurements were performed under pulsed excitation (200ns/100kHz) for 1-mm-long, 100- $\mu\text{m}$ -wide uncoated lasers mounted epi-side up onto gold coated copper blocks.

Favorable reduction of the beam divergence eventually brings unfavorable degradation of the laser parameters for the structure 5. Threshold current increases up to 300 mA and  $T_0$  decreases down to 50 K. Lasers with structures 3 and 4 demonstrate fast axis beam divergences below 50 and 45 degrees, respectively, and do not experience other parameter degradation. Twofold increase of the threshold current density in lasers with waveguide core width of 250 nm can be explained by: (a) reduction of the coupling between double-QW active region and laser mode; (b) modal leakage into high-index GaSb substrate. Both (a) and (b) are caused by spreading of the optical field into direction of n-cladding. Double-QW optical confinement factor gets decreased gradually since mode occupies bigger volume and its maximum shifts from waveguide core center. Eventually, waveguide core width can be reduced below cut-off value (estimated to be about 150 nm) and no mode could be supported. Progressing increase of the field amplitude in

the n-cladding would necessitate increase of the n-cladding thickness when decreasing core width to prevent modal leakage into the substrate. Reduction of the optical confinement, increase of the internal optical loss as well as modal leakage into the substrate was identified from modal gain spectral measurements.

Modal gain spectra were measured for multimode diode lasers using Hakki-Paoli method supplemented by the spatial filtering optics. Figure 8 plots selected spectra obtained at several under threshold currents for diode lasers with structures 1, 3, 4 and 5.

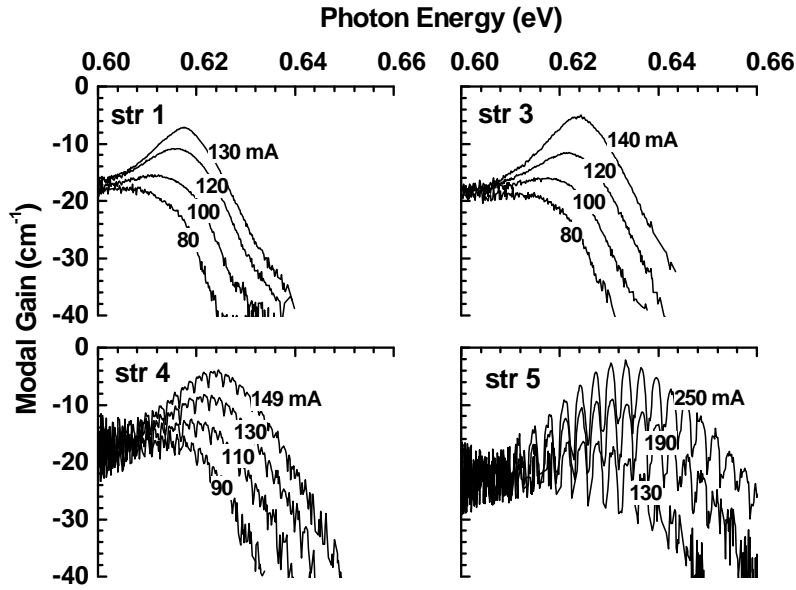


**Figure 8.** Modal gain spectra measured at several under threshold currents for 1-mm-long, 100- $\mu\text{m}$ -wide uncoated lasers. Structure numbers correspond to table 1.

Values of the internal optical losses can be estimated to be  $5 - 6 \text{ cm}^{-1}$  for structures with 850, 550 and 350 nm wide waveguide cores. Indeed, no increase of the internal optical loss is expected if the overlap of the optical field with p-cladding does not increase in asymmetric narrow waveguide laser heterostructures. However, the internal optical loss in structure 5 does increase up to  $8 - 10 \text{ cm}^{-1}$ . The loss increase is also accompanied by pronounced periodic modulation of the modal gain spectra. The modulation is indication of the strong modal leakage into the substrate despite increased n-cladding thickness up to 2500 nm. The slight hint of the modulation can be seen in gain spectra for structure 4 implying that the cladding thickness should have been increased in lasers with 350 nm core already.

Figure 9 plots current dependencies of the peak modal gain for structures 1, 3, 4 and 5. Transparency current is 90 - 100 mA regardless of laser waveguide heterostructure geometry. Indeed, the devices with identical double-QW active regions are expected to have very similar transparency currents unless injection efficiency changes with waveguide core width. Differential gain with respect to current is directly proportional to optical confinement factor and thus is expected to be decreasing together with waveguide core width. Marginal (if any) decrease of the differential gain is observed for reduction of the waveguide width from 850nm down to 350 nm. Twofold reduction of the differential gain is observed in structure 5 with core width of 250 nm. Sharp drop of the optical confinement factor with reduction of the waveguide width in

the range of narrow waveguides can account for this observation. Estimated ratio of the confinement factors of structures 1 and 5 is 2 indeed.

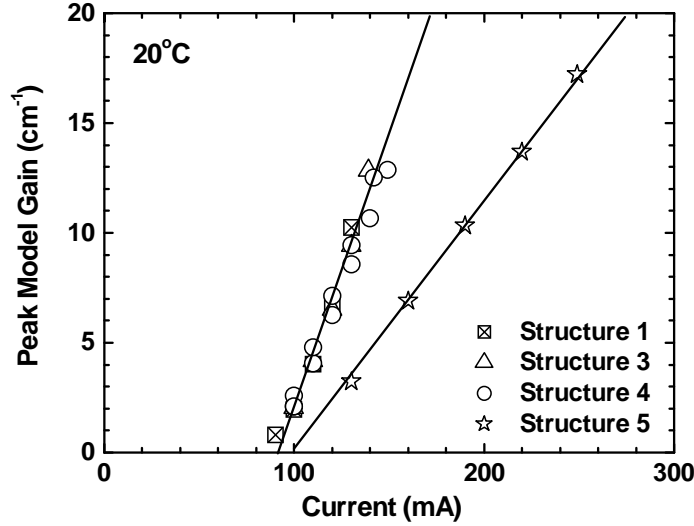


**Figure 9.** Current dependences of the peak modal gain measured for laser with structures 1, 3, 4 and 5.

Measurement of CW output power was performed for diode lasers and their arrays. The devices were indium-soldered epi-side down onto gold-coated copper blocks. The blocks were bolted to thermoelectrically cooled (TEC) copper surface. The heat from the other side of the TEC was removed by flowing water. The stage was able to drive up to 100 W of heat. This capacity was ample for individual lasers but proved insufficient to drive currents in excess of 60A through linear arrays.

Diode lasers with structure 3 (far field divergence with FWHM of 50 degrees) generate above 1.5 W of CW power and demonstrate peak power conversion efficiency in excess of 28 % (Figure 10a).

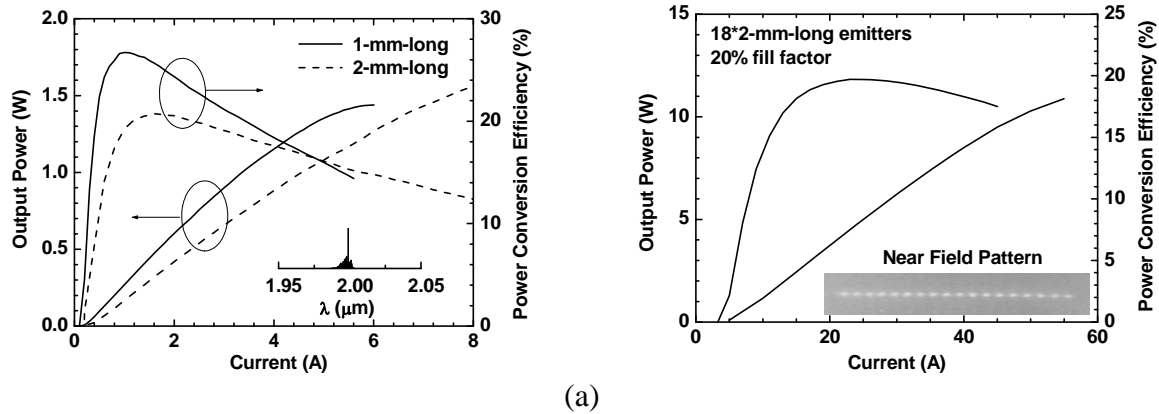


**Figure 10.** (a) CW power and power conversion characteristics measured at 20°C for 1- and 2-mm-long, AR/HR coated lasers with structure 3. Inset shows laser spectrum. (b) CW power and power conversion characteristics measured at 20°C for 2-mm-long, AR/HR coated 18-element linear laser array with structure 3. The array fill-factor was 20%, i.e. 100-μm-wide emitters with 500-μm pitch. The inset shows the corresponding near field.

Linear laser array with fill factor of 20% composed of eighteen 2-mm-long emitters generated above 11 W at 20°C at current of 55 A (Figure 10b). Power conversion efficiency was

above 20 % in peak and above 15 % at maximum power level. Driving current and output power were limited by TEC stage heat removal capabilities.

Diode lasers with structure 4 (far field divergence with FWHM of 44 degrees) generate 1.4 W of CW power but peak power conversion efficiency was below 20 % (Figure 11a). Smaller value of the output power and efficiency is associated with higher optical loss and stronger temperature sensitivity of the threshold. Still the devices were producing more than 1 W of 2  $\mu\text{m}$  power at power conversion efficiency better than 10 %.

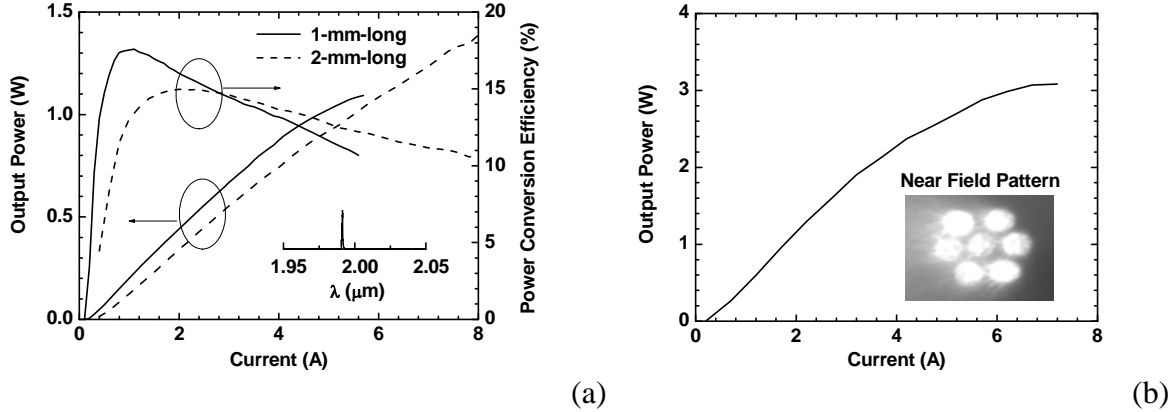


**Figure 11.** (a) CW power and power conversion characteristics measured at 20°C for 1- and 2-mm-long, AR/HR coated lasers with structure 4. Inset shows laser spectrum. (b) Fiber coupled CW power generated by seven 2-mm-long AR/HR coated devices with structure 4. The inset shows the near field image of the fiber bundle output.

Seven 2-mm-long AR/HR coated single emitters of structure 4 were epi-down mounted onto Au-coated BeO blocks and connected in series. Output light was collected by a cylindrical micro-lens in front of each emitter into seven multimode silica fibers (core diameter of 105  $\mu\text{m}$ ). No optimization of the collecting optics was done for the particular 2  $\mu\text{m}$  laser technology. More than 3 W of CW power was collected from the other end of the fiber bundle (Figure 10b).

Figure 12a shows calculated band alignment and near field distribution for 1.95  $\mu\text{m}$  high power diode lasers with asymmetric waveguide and optimized laser heterostructure [11]. The active region contained three 7-nm-wide compressively strained  $\text{In}_{0.25}\text{Ga}_{0.75}\text{Sb}$  quantum wells (QWs) separated by 20-nm-thick  $\text{Al}_{0.3}\text{Ga}_{0.7}\text{As}_{0.03}\text{Sb}_{0.97}$  barriers. The active region was placed into the maximum of the near field distribution. The 360- and 170-nm-thick  $\text{Al}_{0.3}\text{Ga}_{0.7}\text{As}_{0.03}\text{Sb}_{0.97}$  layers separated active region from p- and n-claddings. 1- $\mu\text{m}$ -thick  $\text{Al}_{0.85}\text{Ga}_{0.15}\text{As}_{0.06}\text{Sb}_{0.94}$  p-cladding layer was Be doped to  $10^{17} \text{ cm}^{-3}$  over the 400 nm adjacent to waveguide core and to  $10^{18} \text{ cm}^{-3}$  over the remaining 600 nm. 2500-nm-thick  $\text{Al}_{0.45}\text{Ga}_{0.55}\text{As}_{0.04}\text{Sb}_{0.96}$  n-cladding layer was Te doped to nominal  $10^{18} \text{ cm}^{-3}$ . 20-nm-thick AlSb and 5-nm-thick  $\text{AlAs}_{0.1}\text{Sb}_{0.9}$  layers were inserted between waveguide core and n- and p-cladding layers, respectively.

Current independent far field patterns with beam divergences of 42 and 15 degrees FWHM were measured in fast and slow axis's, respectively (Figure 12b). Low divergence of only 42 degrees was observed in diffraction limited fast axis direction due to enhanced spot size in the corresponding near field. Reduction of the aluminum contents in n-cladding from 85% to 45% was accompanied by undesired reduction of the corresponding valence band offset with core alloy by about 200 meV. To balance the reduced valence band offset the hole stopper layer was introduced. Electron stopper layer was added on p-side to further reinforce carrier confinement in the waveguide core.

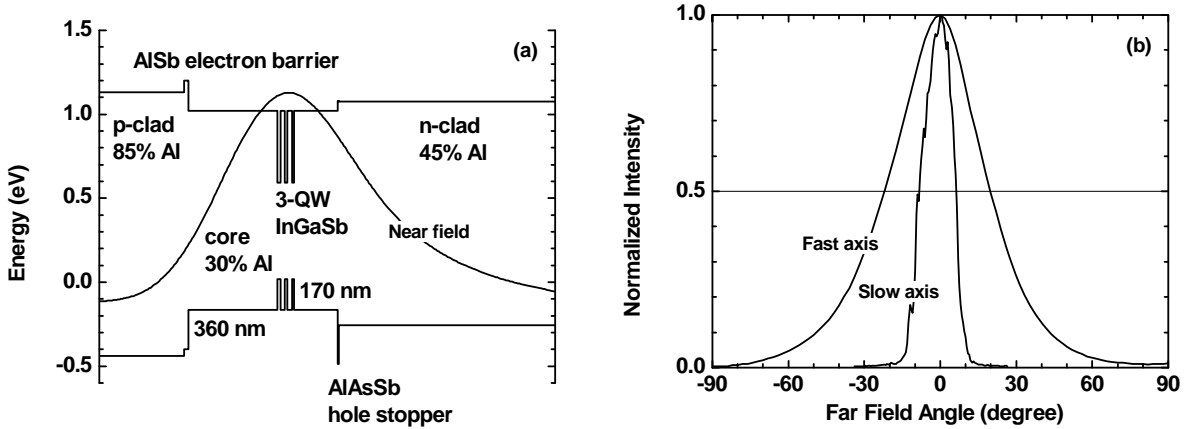


**Figure 12.** (a) Calculated band diagram of the laser heterostructure overlapped with near field distribution; (b) Corresponding far field patterns measured in slow and fast axis directions.

Figure 13 plots the corresponding device power and power conversion characteristics. Maximum CW output power of about 1.45 W were measured for 100- $\mu\text{m}$ -wide 3-mm-long coated lasers at 20  $^{\circ}\text{C}$ . Power conversion efficiency remained above 11 % at maximum output power level. Devices operate at voltages below 1.5 V. Parameters  $T_0 \approx 80$  K and  $T_1 \approx 250$  K characterized exponential temperature dependence of the threshold current and slope efficiency of 1-mm-long uncoated devices in the temperature range from 15 to 50  $^{\circ}\text{C}$ .

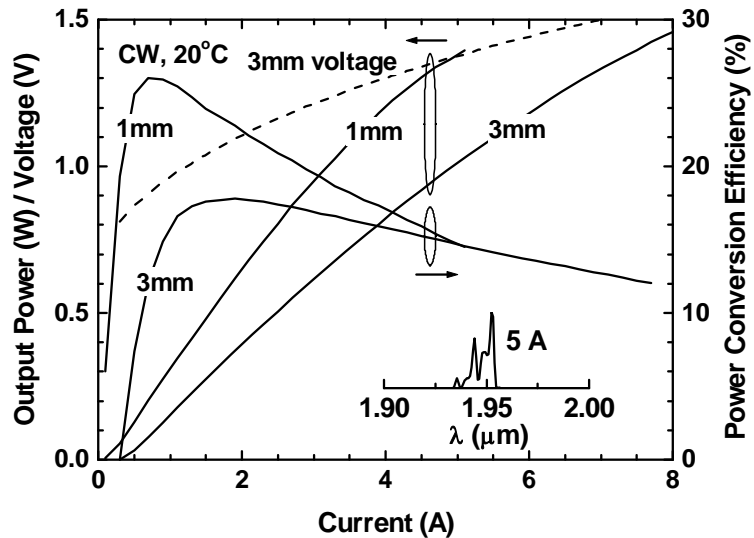


**Figure 13.** CW power and power conversion characteristics of 100- $\mu\text{m}$ -wide 1- and 3-mm-long AR/HR coated devices measured at 20  $^{\circ}\text{C}$ . Inset shows spectrum of 3-mm-long laser at 5 A.

The butt coupling to 0.39 NA 200  $\mu\text{m}$  core silica fiber was performed and efficiency in excess of 65% was demonstrated. Thus the record performance parameters were achieved for 1.95  $\mu\text{m}$  high power diode lasers. The diode lasers with characteristics presented in Figure 11 were utilized for pumping of the Ho-doped fiber laser.

### (b) Resonantly pumped Holmium doped lasers.

The development of the holmium doped fiber lasers was performed in collaboration with Dr. Stuart Jackson (University of Sydney, Australia).

Fibre lasers that emit light at 2.1  $\mu\text{m}$  have drawn a lot of recent interest because of the large number of potential applications that involve the atmospheric transmission window between 2.1 and 2.25  $\mu\text{m}$ . Fibre lasers exploiting the  $^5\text{I}_7 \rightarrow ^5\text{I}_8$  transition of Ho $^{3+}$  offer the most efficient route to high power emission in the 2.1 to 2.2  $\mu\text{m}$  region. To date, the highest power from Ho $^{3+}$ -based fibre lasers has been generated using Tm $^{3+}$  co-doping and diode pumping at  $\sim 790$  nm [12] however the largest slope efficiency has involved pumping the upper laser level directly using high power Tm $^{3+}$ -doped silicate glass fibre lasers [13]. Diode pumping of singly Ho $^{3+}$ -doped fibre lasers at 1150 nm [14] provides a simple laser arrangement and potentially better energy storage; however, the highest slope efficiencies for pumping at this wavelength are approximately 51%. The developments of high power diode lasers emitting at 1.95  $\mu\text{m}$  has opened up the opportunity to diode pump Ho $^{3+}$ -based glass fibre lasers directly into the upper laser level and at the peak of the  $^5\text{I}_7$  absorption in a similar way to Ho:YAG lasers [15]. In addition, the resultant large Stokes limit of 93% allows the use of fibre materials that have weaker thermo-mechanical properties but lower phonon energies compared to the silicate glasses.

Prior to laser development the characterization of holmium doped fluoride glass was performed. The Ho:ZBLAN bulk material was acquired from FiberLabs (Japan). Figure 14 below plots the room temperature absorption and photoluminescence spectra of the Ho:ZBLAN glass (30,000 ppm by mole of Holmium) measured at Stony Brook University. Absorption spectra peaks near 1.95  $\mu\text{m}$  (0.64 eV) while emission peaks near 2.06  $\mu\text{m}$  (0.60 eV). Absorption coefficient is above 1.5  $\text{cm}^{-1}$  in maximum. Indeed nearly 60 % reduction of the 2  $\mu\text{m}$  diode laser power was observed after single pass through 1 cm-long Ho:ZBLAN disk.

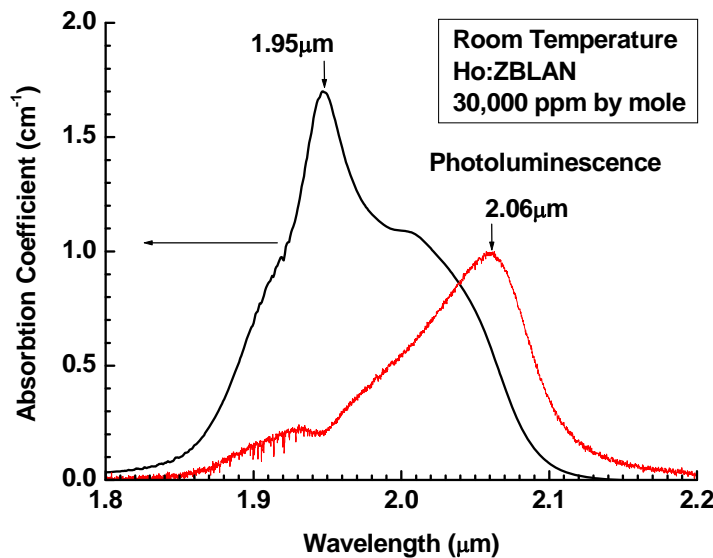


**Figure 14.** Room temperature absorption and emission spectra of 30,000 ppm/mole Ho:ZBLAN material obtained from Fiber Labs.

The experimental arrangement for the  $\text{Ho}^{3+}$ -doped ZBLAN fiber laser is shown in Figure 15. The emission from each high power  $1.94 \mu\text{m}$  diode laser was first collimated using an aspheric ZnSe lens (Lightpath, Orlando) to collimate the fast axis and a cylindrical lens (CVI, New Mexico) to further collimate the slow axis; the total transmission efficiency for the collimating arrangement was 91%. The emission from the two diodes was combined using a polarizing beam splitter (CVI, ~80% transmission) and the pump light focused into the cladding using a standard lens.

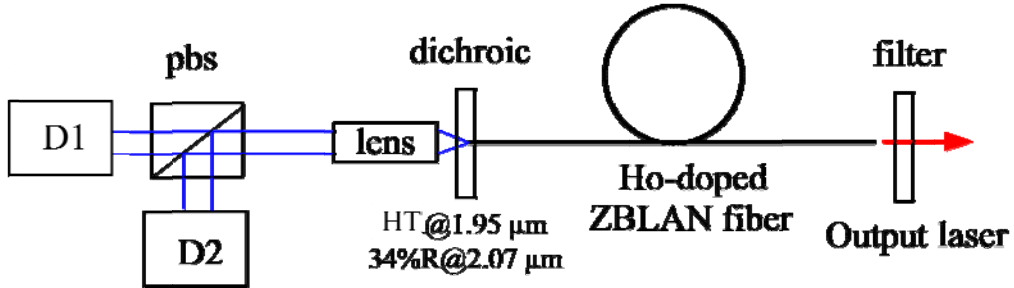


**Figure 15.** Experimental setup of the diode pumped  $\text{Ho}^{3+}$ -doped ZBLAN laser. Pbs represents polarizing beam splitter and D1-D2 represent the two pump diodes.

For the resonator, one highly pump-transmitting dichroic mirror with reflectivity of 34% at  $2.1 \mu\text{m}$  and 90% transmission at  $1.94 \mu\text{m}$  was butted against one end of the fibre; the resonator was completed using the 4% Fresnel fibre end reflection. For the measurements of the laser output, a dichroic mirror with reflectivity of 99% at  $1.94 \mu\text{m}$  and 96.5% at  $2.1 \mu\text{m}$  mirror was used to filter the pump light. An optical spectrum analyzer (Yokogawa AQ6375, Japan) was used to measure the pump and laser spectra. The double-clad  $\text{Ho}^{3+}$ -doped double clad fiber (FiberLabs, Japan) had a  $\text{Ho}^{3+}$  concentration 12 000 ppm and D-shaped pump core with diameter of  $125 \mu\text{m}$  across the circular cross section and numerical aperture (NA) of 0.50. The fiber had a  $10\text{-}\mu\text{m}$ -core diameter and an NA of 0.16 and hence the single mode cutoff wavelength was close  $2.1 \mu\text{m}$ . The low  $\text{Ho}^{3+}$  concentration was chosen to minimize energy transfer between  $\text{Ho}^{3+}$  ions. The absorption coefficient, absorption cross section and launch efficiency were measured to be  $0.60 \text{ m}^{-1}$ ,  $3.9 \times 10^{-25} \text{ m}^2$  and 87% respectively using cutback measurements. The fiber length of 2.0 m provided 73% pump absorption efficiency.

The measured total output power from the fibre laser as a function of the absorbed pump power for both resonator arrangements is shown in Figure 16a. For the cavity involving Fresnel reflection from each end of the fibre, a maximum output power of 348 mW was produced at a slope efficiency of 58%. The threshold pump power was 100 mW owing to the low background loss of the fiber in the  $2.1 \mu\text{m}$  region and long lifetime of the  ${}^5\text{I}_7$  level (~12 ms). For the resonator employing the dichroic mirror, a maximum output power of 516 mW was generated at a slope efficiency of 78%, which was limited by the maximum launched pump power of 707 mW. No thermo-optical problems or output saturation was observed. The threshold pump power of 70 mW was comparatively lower because the dichroic mirror provided 34% reflection. Figure 16b shows the optical spectrum of the output at the maximum pump power for both resonator arrangements. The pump light spectrum (see inset to Figure 16b) comprises of two peaks; one peak from each of the diode lasers. For the Fresnel reflection only resonator, the laser transition operates with a center wavelength of  $2.073 \mu\text{m}$  and bandwidth of 2 nm. When the dichroic mirror was applied, the center wavelength lengthened to  $2.082 \mu\text{m}$  and the bandwidth was kept at 2 nm. The mirror produces a lower threshold for this transition which created more ground state ions and more reabsorption hence forcing the terminating level of the laser transition further up the  ${}^5\text{I}_8$  multiplet.

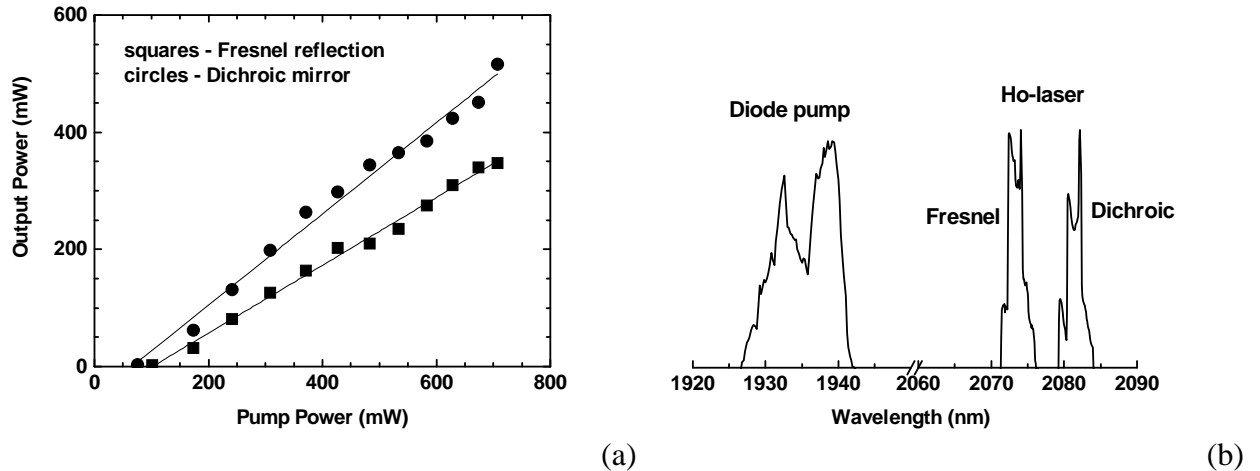


**Figure 16.** (a) Measured total output power from both ends of fiber as a function of the absorbed pump power for the cavity arrangement that employed either Fresnel reflection from the ends of the fiber or the dichroic mirror; (b) Measured spectrum of laser transition for both cavity arrangements at the maximum pump power. The measured spectrum for pump lasers at maximum current is also shown.

The slope efficiency of 78% measured in this demonstration is lower than corresponding efficiencies for core-pumped Ho<sup>3+</sup>-doped silicate glass fibre lasers using Tm<sup>3+</sup>-doped silica fiber lasers as pump sources. The lower efficiency may result from pump light absorption in the polymeric cladding of the fibre.

We have demonstrated what we believe to be the first Ho<sup>3+</sup>-based fibre laser which is diode pumped at 1.94 μm. The fibre laser operated at slope efficiencies comparable to the Stokes limit and further optimization of the laser will involve longer fibres for better absorption efficiency and a Bragg grating that will narrow the bandwidth and provide single sided output.

### (c) Development of the GaSb-based type-I quantum-well diode lasers with longer wavelength.

Diode lasers operating in the spectral region above 2.5 μm are required for a variety of applications. Many important gases and other chemical agents can be remotely detected by tunable laser spectroscopy in this spectral region. For instance, methane, ethane, acetylene, methanethiol, dimethyl sulfide, hydrogen cyanide, etc. absorb strongly between 3 and 4 μm. Analysis of concentrations and isotopic composition of these gasses provides key information on geochemical processes, atmospheric photochemistry, and hydrothermal and biological activity. High power  $\lambda \geq 2.5$  μm beams are required for medical therapy, laser surgery, infrared illumination, countermeasures, etc. Type-I quantum well (QW) diode lasers grown by molecular beam epitaxy on GaSb substrates operate at room temperature in continuous wave mode within the spectral range up to 3.36 μm [16-21]. The devices are in demand for laser spectroscopy, medical diagnostics and therapy, material processing, as well as infrared illumination and countermeasures.

#### (c).1. 2.7 μm GaSb based diode lasers with quinary waveguide.

In previously reported 2.7 μm emitting lasers the waveguide was broadened and made of quaternary AlGaAsSb alloy [18]. In this work we present the results of fabrication and characterization of 2.7 μm GaSb based diode lasers with a new design. The total thickness of waveguide is reduced from 840 nm to 470 nm and quinary AlInGaAsSb alloy is used as a

waveguide/barrier material in place of quaternary AlGaAsSb. The waveguide thickness was optimized for maximum coupling between the optical field and the electrons in QWs. Increased overlap of the laser mode with p-cladding was balanced by reducing doping level in corresponding layer. New devices demonstrated threshold current densities as low as  $200 \text{ A/cm}^2$  (for 2 mm long and 100  $\mu\text{m}$  wide coated lasers) at room temperature in CW operation regime. CW output power of 600 mW and peak power conversion efficiency of 10% were achieved at heatsink temperature of 16°C.

The laser heterostructure was grown by solid-source molecular beam epitaxy using VEECO GEN-930 modular system equipped with valved cracker cells for both arsenic and antimony. The n-cladding layer was 2.0  $\mu\text{m}$  wide  $\text{Al}_{0.85}\text{Ga}_{0.15}\text{As}_{0.06}\text{Sb}_{0.94}$  doped with Te to nominal level of  $10^{18} \text{ cm}^{-3}$  (lower than nominal doping levels are expected in quaternary aluminum-containing alloys). The p-cladding  $\text{Al}_{0.85}\text{Ga}_{0.15}\text{As}_{0.06}\text{Sb}_{0.94}$  layer was Be doped to  $2 \times 10^{17} \text{ cm}^{-3}$  over the first 0.5  $\mu\text{m}$ , and to  $8 \times 10^{17} \text{ cm}^{-3}$  over the remaining 1  $\mu\text{m}$ . Thus the doping level in the p-cladding was decreased compared to the level of  $10^{18} \text{ cm}^{-3}$  used in [18]. Graded bandgap heavily doped transition layers were introduced between the substrate and n-cladding and between the p-cladding and p-cap to assist carrier injection. Nominally undoped quinary  $\text{In}_{0.2}\text{Ga}_{0.6}\text{Al}_{0.2}\text{As}_{0.2}\text{Sb}_{0.8}$  waveguide layer contained two 12 nm wide InGaAsSb QWs in the center. The QWs were separated by 50nm of waveguide material and contained about 47% of indium resulting into compressive strain of 1.7%. The wafer was processed into 100  $\mu\text{m}$  wide gain-guided lasers. For measurement of the device modal gain spectra the 1-mm-long uncoated lasers were mounted epi-up onto Au-coated polished copper blocks. For CW characterization the facets were coated to reflect 3% (AR) and 95% (HR). The devices were In-soldered epi-side down onto Au-coated polished copper blocks.

Figure 17 shows CW light-current and power efficiency characteristics of 2 mm long AR/HR coated devices measured at the coolant temperature of 16°C.

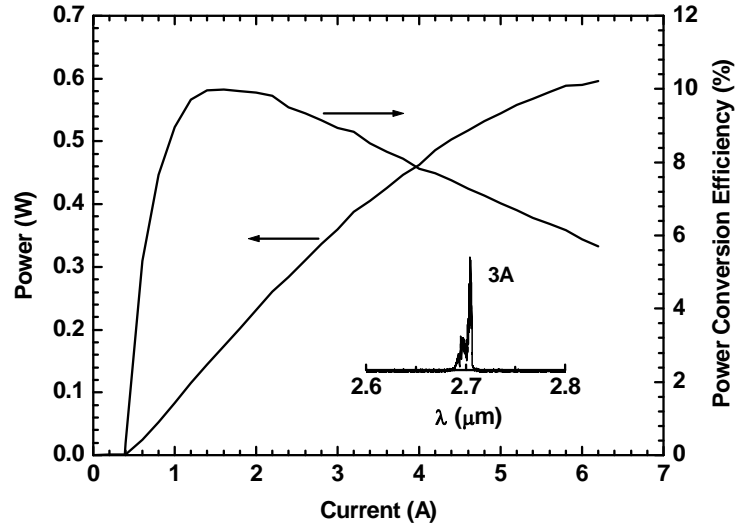


**Figure 17.** CW light-current and power-conversion characteristics of 2.7  $\mu\text{m}$  emitting 2-mm-long AR/HR coated lasers. The inset shows the laser spectrum at 3A.

The measured CW threshold current density was  $200 \text{ A/cm}^2$ , and near threshold external efficiency was 0.32 photons/electron. The maximum output power of 600 mW was achieved at 6.5 A of continuous wave current. The power conversion efficiency peaked at 10% at 1.5 A

current. Improved output power and power conversion efficiency correlate with nearly halved threshold current density ( $200 \text{ A/cm}^2$  versus  $350 \text{ A/cm}^2$ ) and increased external efficiency (32% versus 26%).

The modal gain spectra (Figure 18a) of 1 mm long uncoated device were measured for currents below thresholds using Hakki-Paoli method supplemented by the spatial filtering technique. The total optical loss of  $17 \text{ cm}^{-1}$  was determined from the long wavelength part of the gain spectra. Assuming the distributed mirror loss of  $12 \text{ cm}^{-1}$  for uncoated 1-mm-long devices, the internal optical loss can be estimated as  $5 \text{ cm}^{-1}$ . Calculated overlap of the modal field with p-cladding was about 15% in devices with 470 nm waveguide width (8% for broadened waveguide devices from [18]). Relatively low value of the internal optical loss shows that the selected doping profile was effective in reducing free carrier absorption in the p-cladding layer. The voltage drop across laser heterostructure did not noticeably increase due to lower p-cladding doping and the devices demonstrated less than 1.7 V at 6.5 A of CW current.

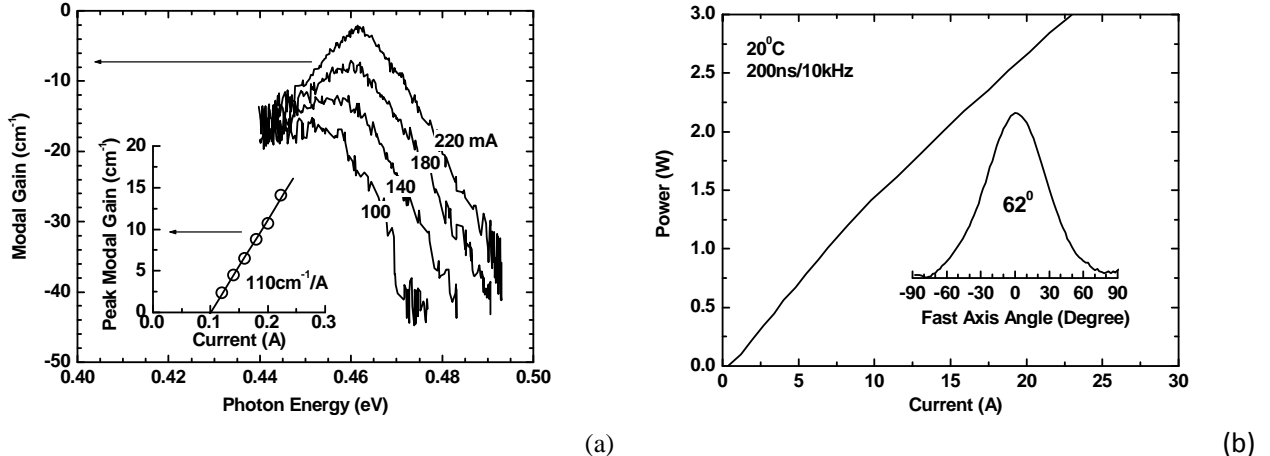


**Figure 18.** (a) Current dependences of the modal gain spectra measured at  $20^\circ\text{C}$  for 1-mm-long uncoated devices. The inset shows the corresponding dependence of the peak modal gain on current; (b) Pulsed light-current characteristics of  $2.7 \mu\text{m}$  emitting 2-mm-long AR/HR coated lasers. The inset shows the fast axis far field divergence measured in CW regime.

The inset in Figure 18a shows the dependence of the peak modal gain on the under-threshold current. The rate of increase of peak modal gain with current is  $110 \text{ cm}^{-1}/\text{A}$  for 1-mm-long 100-μm-wide gain guided devices. The optical confinement factor for QWs is expected to improve by about 30% when the waveguide material is changed from  $\text{Al}_{0.25}\text{Ga}_{0.75}\text{As}_{0.02}\text{Sb}_{0.98}$  to  $\text{Al}_{0.2}\text{In}_{0.2}\text{Ga}_{0.6}\text{As}_{0.2}\text{Sb}_{0.8}$  and the total waveguide thickness is reduced from 840 nm to 470 nm. Increased optical confinement factor should enhance the device differential gain with respect to concentration. Additional improvement of the device differential gain with respect to total device current stems from the fact that thermionic hole delocalization is expected to be mediated by the use of quinary barrier material. Thus, improved hole localization and enhanced optical confinement factor lead to increased device differential gain. Improved differential gain and relatively low internal optical loss result in decreased threshold current density.

Figure 18b shows the light-current characteristics measured in short pulse mode (200ns/10kHz) corresponding to negligible device heating (less than 0.5 W of heat is dissipated on average at the maximum current). More than 3 W peak power was recorded at the current of 25 A. The devices show the fast axis divergence of  $62^\circ$  measured as full-width-at-half-maximum.

Both parameters  $T_0$  and  $T_1$  characterizing thermal sensitivity of the device threshold current and slope efficiency were about 70K measured in temperature range from 20 to 50°C.

Summarizing, 2.7 $\mu$ m type-I GaSb-based laser diodes with quinary AlGaInAsSb waveguide/barrier material were developed and characterized. The devices were fabricated with waveguide width optimized for maximum QW optical confinement. Threshold current density was 100 A/cm<sup>2</sup> per QW. Continuous wave output power of 600 mW was achieved at the heatsink temperature of 16°C and current of 6.5 A. Power conversion efficiency peaked at 10% at the current of 1.5 A. Devices demonstrate superior performance parameters as compared to previously reported 2.7  $\mu$ m emitters having broadened waveguide made of the quaternary AlGaAsSb alloy.

### (c).2. Single Spatial Mode Room Temperature Operated 3.15 $\mu$ m Diode Lasers.

The devices were developed in collaboration with Jet Propulsion laboratory

Single spectral mode diode lasers operating at room temperature in continuous-wave regime and providing mW level output power are required for development of the highly sensitive and compact tunable laser spectroscopy systems. Single mode type-I quantum-well (QW) GaSb-based diode lasers operating near 3 mm were previously reported [22]. The laser heterostructure comprised GaSb binary as a barrier material and corresponding ridge waveguide devices produced 7 mW at 15 C and operated up to 30 C in continuous-wave (CW) regime. In this work we report the design and development of single special mode GaSb-based type-I QW diode lasers employing quinary barrier material and operating in the spectral range near 3.15  $\mu$ m. The ridge waveguide diode lasers produced 9 mW of CW output power at 3.16  $\mu$ m at 15 C and had operating wavelength above 3.2  $\mu$ m at 40 C.

The mid-infrared laser heterostructures were grown by solid-source molecular beam epitaxy. In the laser active region there were three 1.65% compressively strained, 14-nm-wide, 40-nm-spaced InGaAsSb QW with nominal indium composition of 52%. Quinary Al<sub>0.20</sub>Ga<sub>0.55</sub>In<sub>0.25</sub>As<sub>0.24</sub>Sb<sub>0.76</sub> random alloy was utilized for barrier and waveguide. The width of the waveguide core from n-cladding to p-cladding was about 1120nm. The n- and p-claddings were Al<sub>0.85</sub>Ga<sub>0.15</sub>As<sub>0.07</sub>Sb<sub>0.93</sub> doped with tellurium and beryllium, respectively. Doping level of the part of the p-cladding layer adjacent to waveguide was kept around 2\*10<sup>17</sup> cm<sup>-3</sup> to reduce internal losses associated with free hole absorption.

For initial material characterization the part of the wafer was processed into multimode gain-guided lasers by opening 100- $\mu$ m-wide windows in the dielectric followed by flat metallization. No etching was performed at this stage to facilitate either optical or electrical lateral confinement. Laser mirrors were cleaved. Uncoated 1-mm-long lasers were mounted epi-side up for pulsed measurements. Figure 19 plots the light-current characteristics measured for minimum thermal penalty in short pulse regime at different heatsink temperatures. The threshold current increases from below 200 mA to above 1 A when device operating temperature increases from 200 K to 290 K. The corresponding decrease of the laser slope efficiency is more than twofold. Strong temperature sensitivity of the lasers slope efficiency contributes to thermally activated increase of the laser threshold current. Pour thermal stability of the laser external efficiency can originate either from internal optical loss increase or reduction of the injection efficiency with temperature. Unless free carrier absorption in active QWs is a dominant loss mechanism and/or QW carrier concentration is not pinned at threshold neither of these effects are fundamental and, hence, temperature stability of laser threshold can be improved.

The measurement of the fast axis far field distribution yielded divergence of 65 - 70 degrees full-width-at-half-maximum (FWHM). The calculations using cladding refractive index of 3.2 [9] and waveguide refractive index guess of 3.8 produced far field distribution with FWHM near 66 degrees. Hence, one can conclude that the 3.8 is descent approximation for quinary alloy refractive index and can be used for ridge waveguide design calculations.

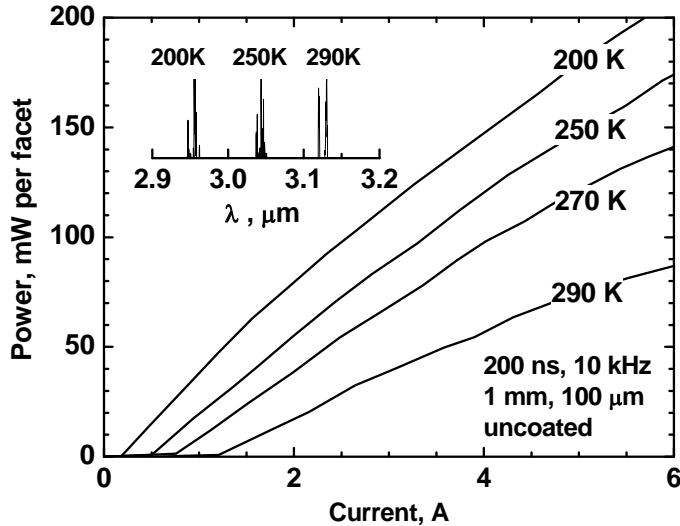


**Figure 19.** Temperature dependence of the short pulse (200 ns, 10 kHz) light-current characteristics for 1-mm-long, 100- $\mu\text{m}$ -wide, uncoated lasers. Inset shows the laser spectra.

Ridge waveguide lasers were fabricated using inductively coupled plasma (ICP) reactive ion etching technique at Jet Propulsion Laboratory. The etching was stopped at 350 - 400  $\mu\text{m}$  before the end of the p-cladding to form shallow 12- $\mu\text{m}$ -wide ridge lasers (Figure 20a).

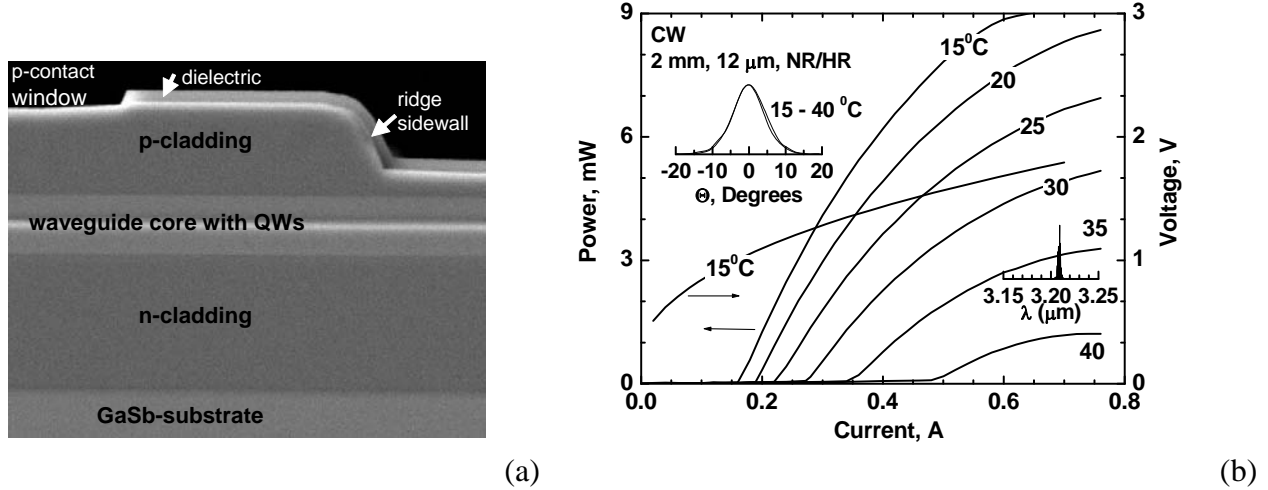


**Figure 20.** (a) SEM image of the front facet section the ridge waveguide laser; (b) CW light-current-voltage characteristics measured for 12- $\mu\text{m}$ -wide 2-mm-long ridge waveguide lasers in temperature range from 15 to 40  $^{\circ}\text{C}$ . Inset shows the slow axis far field distributions measured at 15 and 40  $^{\circ}\text{C}$ . Laser spectrum at 0.4 A of CW current at 35  $^{\circ}\text{C}$  at heatsink is also shown.

Estimated lateral effective index step was about 0.0013. For such a small refractive index step the 12- $\mu\text{m}$ -wide ridge waveguide is expected to support only fundamental mode. The ridge lasers

were cleaved to form 2-mm-long cavities and coated to reflect about 30% (neutral-reflection) and above 90% (high-reflection), respectively. The devices were indium-soldered epi-side down on gold-coated polished copper blocks and characterized. Figure 20b shows the light-current-voltage characteristics and slow axis far field distribution measured at different temperatures. Lasers operate in continuous wave regime up to 40 °C with diffraction limited output beam. The slow axis far field distribution remains nearly unchanged in temperature range from 15 to 40 °C. The measured FWHM is between 9 and 10 degrees. Model calculation predicted the FWHM about 9.4 degrees for a given ridge etch. The maximum power of 9 mW near 3.18 μm was achieved at the current of 0.65A at heatsink temperature of 15°C. The devices generate above 1 mW of CW power at heatsink temperature of 40°C (the operating wavelength is above 3.2 μm, see inset to Figure 20b). The CW threshold current density was about 700 A/cm<sup>2</sup> at 15°C and it rising up to 2 kA/cm<sup>2</sup>. The voltage drop across laser heterostructure was below 2 V at the maximum output power level.

## References

- 1 S. Simanowski, N. Herres, C. Mermelstein, R. Kiefer, J. Schmitz, M. Walther, et al., "Strain adjustment in (GaIn)(AsSb)/(AlGa)(AsSb) QWs for 2.3-2.7 μm laser structures", *J. Crystal Growth*, Vol. 209, p.15, 2000.
- 2 J. Chen, D. Donetsky, L. Shterengas, M. Kisim, G. Kipshidze, G. Belenky, "Effect of Quantum Well Compressive Strain Above 1% On Differential Gain and Threshold Current Density in Type-I GaSb-Based Diode Lasers", *IEEE J. Quantum Electron*, Vol. 44, p. 1204, 2008.
- 3 R. Liang, J. Chen, G. Kipshidze, D. Westerfeld, L. Shterengas, G. Belenky, "High-power 2.2-μm diode lasers with heavily strained active region", *IEEE Photon. Technol. Lett.* 23, 603 (2011).
- 4 B.W. Hakki, T.L. Paoli, "Gain spectra in GaAs double-heterojunction injection lasers," *J. Appl. Phys.* 46, 1299 (1975).
- 5 M. Rattunde, J. Schmitz, G. Kaufel, M. Kelemen, J. Weber, J. Wagner, "GaSb-based 2.x μm quantum-well diode lasers with low beam divergence and high output power", *Appl. Phys. Lett.* 88, 081115 (2006).
- 6 B.S. Ryvkin, E.A. Avrutin, "Nonbroadened asymmetric waveguide diode lasers promise much narrower far fields than broadened symmetric waveguide ones", *J. Appl. Phys.* 98, 026107 (2005).
- 7 A. Chandola, R. Pino and P. S. Dutta, "Below bandgap optical absorption in tellurium-doped GaSb", *Semicond. Sci. Technol.* 20, 886 (2005).
- 8 Z.G. Li, G.J. Liu, M. H. You, L. Li, M. Li, Y. Wang, B. S. Zhang, X.H. Wang, "2.0 μm room temperature CW operation of InGaAsSb/AlGaAsSb laser with asymmetric waveguide structure," *Laser Phys.* 19, 1230 (2009).
- 9 C. Alibert, M. Skouri, A. Joullie, M. Benouna, S. Sadiq, "Refractive indices of AlSb and GaSb-lattice-matched Al<sub>x</sub>Ga<sub>1-x</sub>As<sub>y</sub>Sb<sub>1-y</sub> in the transparent wavelength region", *J. Appl. Phys.* 69, 3208 (1991).
- 10 J. Chen, G. Kipshidze, L. Shterengas, "High-power 2 μm diode lasers with asymmetric waveguide", *IEEE J. Quantum Electron.* 46, 1464 (2010)
- 11 J. Chen, G. Kipshidze, L. Shterengas, "Diode lasers with asymmetric waveguide and improved beam properties", *Appl. Phys. Lett.* 96, 241111 (2010).
- 12 S.D. Jackson, A. Sabella, A. Hemming, S. Bennetts, D.G. Lancaster, "High-power 83 W holmium-doped silica fiber laser operating with high beam quality," *Opt. Lett.* 32, 241 (2007).
- 13 S.D. Jackson, "Midinfrared holmium fiber lasers," *IEEE J. Quantum. Electron.* 42, 187 (2006); A. Guhur, S.D. Jackson, "Efficient holmium-doped fluoride fiber laser emitting 2.1 μm and blue upconversion fluorescence upon excitation at 2 μm", *Opt. Exp.* 18, 20164 (2010)
- 14 S.D. Jackson, F. Bugge, G. Erbert, 'High-power and highly efficient diode-cladding-pumped Ho<sup>3+</sup>-doped silica fiber lasers', *Opt. Lett.* 32, 3349 (2007).

- 
- 15 C.D. Nabors, J. Ochoa, T.Y. Fan, A. Sanchez, H.K. Choi, G.W. Turner, “Ho-YAG laser pumped by 1.9- $\mu$ m diode lasers,” IEEE J. Quantum Electron. 31, 1603 (1995).
16. D.Z. Garbuзов, H. Lee, V. Khalfin, R. Martinelli, J.C. Connolly, G.L. Belenky, “2.3-2.7  $\mu$ m room temperature CW operation of InGaAsSb/AlGaAsSb broad waveguide SCH-QW diode lasers”, IEEE Photon. Technol. Lett. 11, 794 (1999).
17. M. Grau, C. Lin and M.C. Amann, “Low threshold 2.72  $\mu$ m GaInAsSb/ AlGaAsSb multiple-quantum-well laser”, Electronics Letters 38, 1678 (2002).
18. J.G. Kim, L. Shterengas, R.U. Martinelli, G.L. Belenky, “High-power room temperature continuous wave operation of 2.7 and 2.8  $\mu$ m In(Al)GaAsSb/GaSb diode lasers”, Appl. Phys. Lett. 83, 1926 (2003).
19. M. Grau, C. Lin, O. Dier, C. Lauer, and M. -C. Amann, “Room-temperature operation of 3.26  $\mu$ m GaSb-based type-I lasers with quaternary AlGaInAsSb barriers,” Appl. Phys. Lett. 87, 241104, (2005).
20. T. Hosoda, G. Belenky, L. Shterengas, G. Kipshidze, and M. V. Kisim, “Continuous-wave room temperature operated 3.0  $\mu$ m type I GaSb-based lasers with quaternary AlInGaAsSb barriers”, Appl. Phys. Lett. 92, 091106 (2008).
21. L. Shterengas, G. Belenky, T. Hosoda, G. Kipshidze, S. Suchalkin, “Continuous wave operation of diode lasers at 3.36  $\mu$ m at 12 degrees C”, Appl. Phys. Lett. 93, 011103 (2008).
- 22 T. Lehnhardt, M. Hummer, K. Roßner, M. Muller, S. Hofling, A. Forchel, ‘Continuous wave single mode operation of GaInAsSb/GaSb quantum well lasers emitting beyond 3  $\mu$ m’, Appl. Phys. Lett., 2008, 92, p. 183508

## **Supported Personnel**

Dr. L. Shterengas, Assistant professor, PI/PD

Dr. G. Kipshidze, Senior research scientist, MBE growth

J. Chen, Graduate student

PhD in EE May 2011, employed by Crystal IS, Inc. (Green island, NY 12183)

## **Collaborations**

1. Fiber laser development: Dr. Stuart Jackson, University of Sydney, Australia

2. Ridge waveguide 3  $\mu\text{m}$  lasers development: Dr. S. Forouhar, Jet Propulsion Lab

## **Material Transfer Agreement**

Executed between Stony Brook University and University of Sydney to deliver pumping diodes for resonant pumping of holmium doped fiber laser.

## **Dissertations**

Dr. J. Chen, "Development of Type-I GaSb-based Diode Lasers and Arrays Operating within Spectral Range above 2 $\mu\text{m}$ ", Stony Brook University, Department of Electrical and Computer Engineering, May 2011.

## **Publications**

### **Book Chapter**

G. Belenky, L. Shterengas, M. Kisin, T. Hosoda, "GaSb-based type-I quantum well diode lasers" in "Semiconductor lasers - fundamentals and applications", Woodhead Publishing, to be published in (2011).

### **Scientific Journals**

1. R. Li, J. Li, L. Shterengas, S.D. Jackson, "Highly efficient holmium fibre laser diode pumped at 1.94  $\mu\text{m}$ ", Electron. Lett. Accepted, August 25 (2011).
2. R. Liang, J. Chen, G. Kipshidze, D. Westerfeld, L. Shterengas, G. Belenky, "High-power 2.2- $\mu\text{m}$  diode lasers with heavily strained active region", IEEE Photon. Technol. Lett. 23, 603 (2011).
3. J. Chen, G. Kipshidze, L. Shterengas, "High-power 2  $\mu\text{m}$  diode lasers with asymmetric waveguide", IEEE J. Quantum Electron. 46, 1464 (2010)
4. J. Chen, G. Kipshidze, L. Shterengas, "Diode lasers with asymmetric waveguide and improved beam properties", Appl. Phys. Lett. 96, 241111 (2010).
5. J. Chen, T. Hosoda, G. Kipshidze, L. Shterengas, G. Belenky, A. Soibel, C. Frez. S. Forouhar "Single spatial mode room temperature operated 3.15  $\mu\text{m}$  diode lasers", Electron. Lett. 46, 367 (2010).
6. J. Chen, G. Kipshidze, L. Shterengas, T. Hosoda, Y. Wang, D. Donetsky, G. Belenky "2.7  $\mu\text{m}$  GaSb based diode lasers with quinary waveguide", IEEE Photon. Technol. Lett. 21, 1112 (2009).